nature cell biology

The kinesin-14 Klp2 organizes microtubules into parallel bundles by an ATP-dependent sorting mechanism

Marcus Braun[1], Douglas R. Drummond[2], Robert A. Cross[2] and Andrew D. McAinsh[1,3]

The dynamic organization of microtubules into parallel arrays allows interphase cells to set up multi-lane highways for intracellular transport and M-phase cells to build the mitotic and meiotic spindles. Here we show that a minimally reconstituted system composed of Klp2, a kinesin-14 from the fission yeast *Schizosaccharomyces pombe*, together with microtubules assembled from purified *S. pombe* tubulin, autonomously assembles bundles of parallel microtubules. Bundles form by an ATP-dependent sorting mechanism that requires the full-length Klp2 motor. By this mechanism, antiparallel-overlapped microtubules slide over one another until they dissociate from the bundles, whereas parallel-overlapped microtubules are selectively trapped by an energy-dissipating force-balance mechanism. Klp2-driven microtubule sorting provides a robust pathway for the organization of microtubules into parallel arrays. *In vivo* evidence indicates that Klp2 is required for the proper organization of *S. pombe* interphase microtubules into bipolar arrays of parallel-overlapped microtubules[1–4], suggesting that kinesin-14-dependent microtubule sorting may have wide biological importance.

In eukaryotic mitosis and meiosis, the interlocking half-spindles are each composed of parallel microtubules[5], while in interphase, cells use parallel arrays of microtubules both as stable tracks for motorized intracellular transport and as a guidance system for cell growth and motility[6]. The mechanisms by which cells organize microtubules into parallel arrays are unclear. In principle, parallel arrays might form either by the crosslinking of a set of parallel microtubules emanating from a common organizing centre, or by the capture, orientation and linking-in of individual free microtubules by microtubule-associated proteins and microtubule-attached molecular motors, independently of microtubule dynamics[7–9]. A useful model system for studying the formation of higher-order microtubule-based structures is the interphase microtubule array (IMA) in the fission yeast *S. pombe*. The IMA, which is involved in determining and maintaining cell polarity in fission yeast[10,11], consists of several bundles of parallel microtubules lying parallel to the long axis of the cell. These parallel bundles are linked to one another in a narrow zone of anti-parallel overlap in the centre of the cell[12,13], so that in each half of the cell, dynamic microtubule plus ends grow outwards towards the cell ends. *In vivo,* the IMA grows either from interphase microtubule nucleation centres that are associated with the nucleus, or from secondary nucleation sites in the cytoplasm or on the side of existing microtubules[2,3]. Microtubules that originate from these secondary sites are subsequently recruited into the IMA. These studies demonstrate that a combination of cytoplasmic nucleation factors, stabilizing factors and the Klp2 motor, are required for self-organization of the IMA[1–4]. Here we show that purified, full-length Klp2 alone is sufficient to drive ATP-dependent *in vitro* self-organization of *S. pombe* microtubules into parallel arrays.

Purified, recombinant full-length Klp2 (Fig. 1b) is present in solution at physiological ionic strength (PEM100 buffer (100 mM Pipes pH 6.9, 1 mM $MgCl_2$, 2 mM EGTA) plus 100 mM NaCl) as a single elongated homodimeric species (Fig. 1d, e), consistent with the carboxy-terminal motor domain and amino-terminal flexible tail region being connected by a predicted coiled coil (Fig. 1c). In microtubule gliding assays using microtubules assembled from pig brain tubulin (Fig. 1f), Klp2 drove minus-end-directed motility, as expected for a kinesin-14 family member (Supplementary Information, Movie 1). Gliding velocities were slightly faster with pig brain microtubules (65 ± 1.0 nm s^{-1}; mean ± s.e.m., $n = 50$), compared with microtubules that were assembled from tubulin purified from *S. pombe* (42 ± 0.8 nm s^{-1}; mean ± s.e.m., $n = 50$; Fig. 1h). This slightly slower rate compared with measurements made in *S. pombe* cells (92 nm s^{-1}; ref. 4) probably reflects the involvement of additional regulatory factors *in vivo*. The solution Klp2 ATPase was activated 15-fold more effectively by *S. pombe* microtubules (V_{max} 3.8 ± 0.3 s^{-1}) than by pig brain microtubules (V_{max} 0.25 ± 0.03 s^{-1}) although the apparent affinities for the two microtubule species were similar (K_m for *S. pombe* microtubules = 0.77 ± 0.2 μM and for pig-brain microtubules = 0.55 ± 0.2 μM; Fig. 1i). The origins of the low V_{max} measured for activation of the Klp2 ATPase by pig brain microtubules are currently unclear. Pig brain and *S. pombe* tubulin both caused a modest activation of the Klp2 ATPase (Fig. 1i)[14]. Overall, these experiments demonstrate that our purified full-length Klp2 is an active molecular motor protein.

[1]Chromosome Segregation Laboratory and [2]Molecular Motors Laboratory, Marie Curie Research Institute, The Chart, Oxted, RH8 0TL, Surrey, UK.
[3]Correspondence should be addressed to A.D.M (e-mail: a.mcainsh@mcri.ac.uk)

Received 20 January 2009; accepted 24 February 2009; published online 10 May 2009; DOI: 10.1038/ncb1878

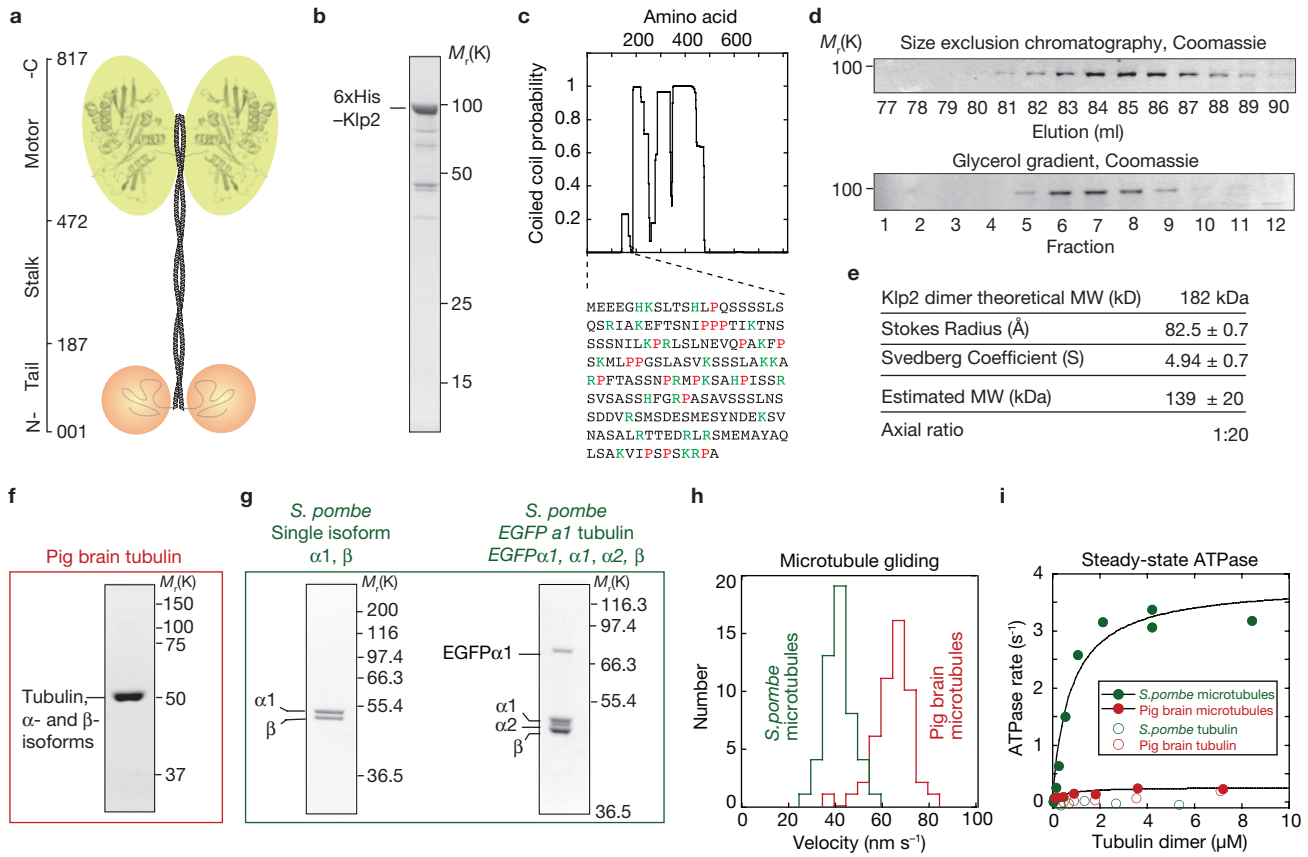

Figure 1 Purified full-length *S. pombe* kinesin-14 Klp2 is a microtubule-minus-end directed motor. (**a**) Schematic of the Klp2 domain structure indicating the motor domain position (based on crystal structure of the Kar3 motor domain[20], coiled-coil and flexible tail region. (**b**) Coomassie-stained SDS–PAGE of purified, recombinant full-length Klp2 protein expressed in *Escherichia coli*. (**c**) Coiled coil prediction of the full-length Klp2 protein using the COILS program[21]. (**d**) Hydrodynamic analysis of the purified full-length Klp2 protein performed in PEM100 buffer plus 100 mM NaCl. The upper panel shows fractions from size exclusion chromatography column and the lower panel fractions from a 5–40% glycerol gradient (**e**) Calculation of hydrodynamic parameters based on the experimentally derived stokes radius and Svedberg coefficients for full-length Klp2. (**f**, **g**) SDS–PAGE and Coomassie staining of purified pig brain tubulin (**f**), single isoform *S. pombe* tubulin (**g**, left panel) and EGFP–α1-tubulin (**g**, right panel). (**h**) Microtubule gliding velocities promoted by Klp2 at 25 °C in 100 mM PIPES buffer containing 100 mM NaCl, 1 mM ATP, 20 μM paclitaxel and 1 mM GMP–CPP, using microtubules polymerized from *S. pombe* EGFP–tubulin (green) and rhodamine labelled pig-brain tubulin (red). (**i**) Steady-state ATPase activity of Klp2 at 25 °C in PEM100, 100 mM NaCl, 1 mM ATP, 20 μM paclitaxel and 1 mM GMP–CPP using non-labelled microtubules polymerized from *S. pombe* tubulin (solid green circles; V_{max} 3.8 ± 0.3 s^{-1}, K_m 0.8 ± 0.2 μM) and pig brain tubulin (solid red circles; V_{max} 0.25 ± 0.03 s^{-1}, K_m 0.5 ± 0.2 μM). The V_{max}/K_m values of 4.75 μM s^{-1} for *S. pombe* and 8.3 μM s^{-1} for pig brain microtubules indicate strongly that Klp2 is a non-processive kinesin[22]. Measurements for non-polymerized *S. pombe* (open green circles) and pig brain tubulin (open red circles) show that the Klp2 kinesin is activated by polymerized microtubules exclusively. Full scans of the SDS–PAGE gels are provided in Supplementary Information, Figs S2, S3.

On the basis of previous experiments with *Drosophila melanogaster* kinesin-14 (Ncd)[15,16], we predicted that the flexible, proline-rich, basic N-terminal tail of Klp2 (theoretical pI 10.0; Fig. 1c) might act as a second microtubule-binding site. To investigate this possibility, we expressed and purified a Klp2 protein lacking the motor domain (Klp2-tail) and a Klp2 protein containing only the motor domain and a short coiled coil to mediate dimerization (Klp2-motor) which was confirmed to exist as a single homodimeric species by size exclusion chromatography, Fig. 2a; Supplementary Information, Fig. S1a). We first demonstrated that full-length Klp2 bound *S. pombe* microtubules in a pelleting assay in the presence of ATP using PEM100 plus 100 mM NaCl buffer (Fig. 2c). This binding was reduced when the experiment was performed using pig brain microtubules (Fig. 2c, compare lanes 2 and 4). Klp2-motor, which lacks the tail domain did not pellet with pig brain microtubules (Fig. 2d, lane 4), indicating that the Klp2 tail greatly increases the microtubule affinity of the motor, and suggesting that the tail contributes a second microtubule binding site. To confirm this, we carried out microtubule pelleting assays with Klp2-tail, which was found to bind both *S. pombe* and pig brain microtubules (Fig. 2e, compare lanes 4 and 10). Thus, only full-length Klp2, with intact tail and motor domains, shows selective binding of *S. pombe* versus pig brain microtubules. Binding of Klp2-tail, to both *S. pombe* and pig brain microtubules, was probably mediated through electrostatic interactions, as pelleting decreased as the ionic strength was increased (Fig. 2e, f). We next determined the stoichiometry of Klp2-tail:*S. pombe* microtubule binding by titration of Klp2-tail using a constant microtubule concentration. This showed stoichiometric binding to the lattice, with saturation at a ratio of about 1:1 Klp2-tail:tubulin heterodimer and a fitted K_d of 1.2 ± 0.1 μM (Fig. 2g, h). These binding data confirm that full-length Klp2 has two independent microtubule-binding sites, one in its head and one in its tail. The specific 1:1 binding of the isolated Klp2-tail domain to microtubules

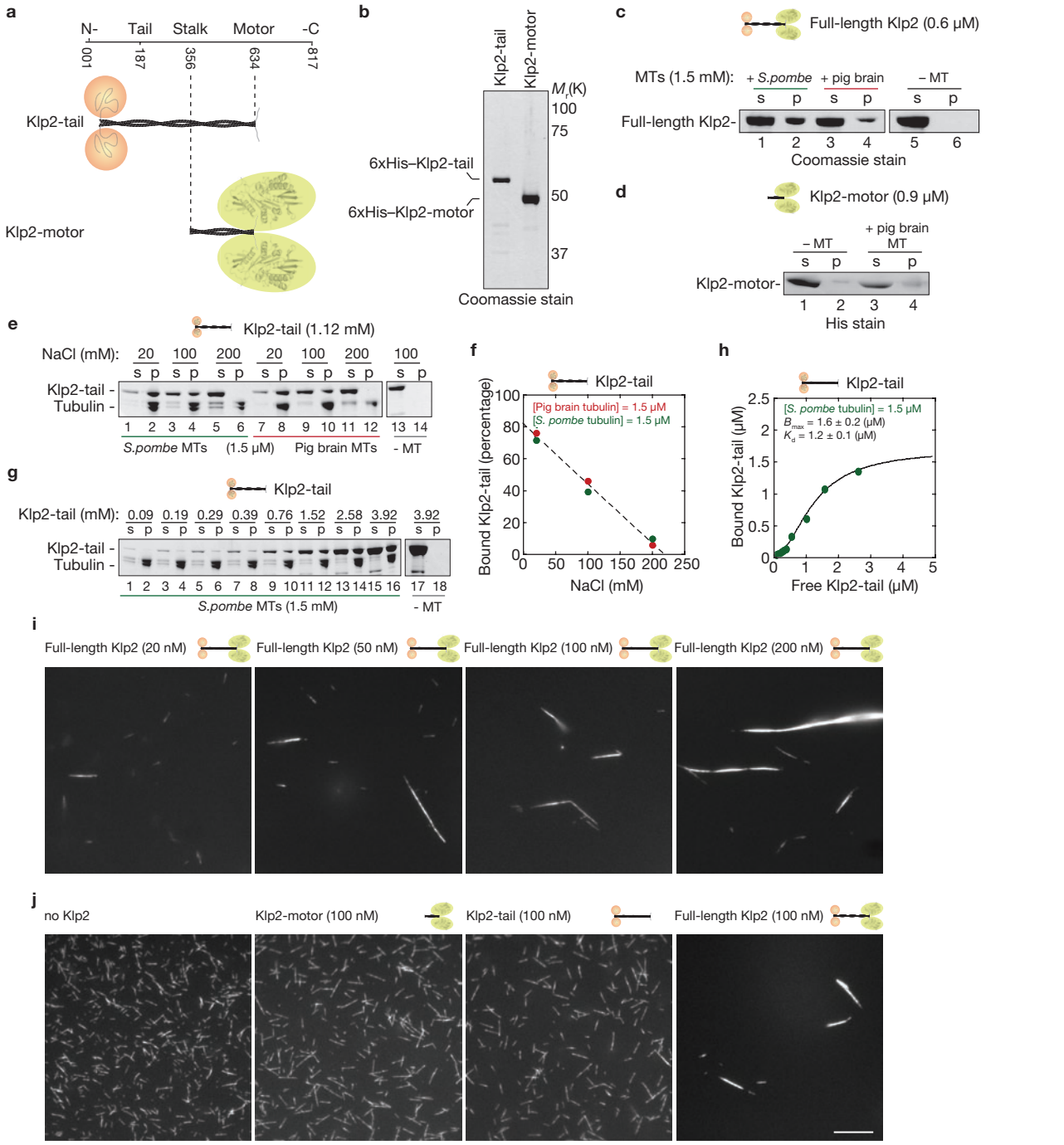

Figure 2 Microtubule bundling requires both the motor-domain and the N-terminal tail region of Klp2. (**a**) Schematic of the Klp2-tail and Klp2-motor constructs. (**b**) Coomassie-stained SDS–PAGE of purified, recombinant Klp2-tail and Klp2-motor proteins expressed in *E. coli*. (**c**, **d**) Microtubule (MT) co-pelleting assay performed in PEM100, 100 mM NaCl, 10 mM β-mercaptoethanol buffer, 1 mM GMP–CPP 1 mM ATP using 0.6 μM of Klp2 and 1.5 μM of non-labelled *S. pombe* (**c**, lanes 1 and 2) or pig brain (**c**, lanes 3 and 4) microtubules, or 0.9 μM Klp2-motor and 1.5 μM pig-brain microtubules. Supernatant (S) and pellet (P) fractions are indicated. (**e**) Binding of Klp2-tail (1.12 μM) to 1.5 μM of *S. pombe* (lanes 1-6) or 1.5 μM of pig brain (lanes 7-12) microtubules in PEM100 plus 20, 100 or 200 mM NaCl. (**f**) Quantification of binding shown in **e**. (**g**) Binding of Klp2-tail (concentrations, 0.1–3.9 μM) to 1.5 μM of *S. pombe* in PEM100 plus 100 mM NaCl. (**h**) Quantification of binding shown in **g**. (**i**) Full-length Klp2 (20–200 nM) was mixed with 200 nM of *S. pombe* EGFP–microtubules (PEM100 plus 100 mM NaCl, pH6.8) and the mixture added to a flow cell. Representative images of the microtubule-motor structures that formed after 20 min are shown. Scale bar, 10 μm. (**j**) Full-length Klp2, Klp2-motor or Klp2-tail (all at 100 nM) were mixed with 200 nM of *S. pombe* EGFP–microtubules and the mixture added to a flow cell. Representative images of the microtubule-motor structures that formed after 20 min are shown. We note that surface binding is mediated by the population of Klp2 that was not microtubule-bound (see pelleting assay, **c**, lane 1), in addition to motors attached to the bundles. For the no motor control and Klp2-tail experiments, *Drosophila* kinesin-1 was pre-bound to the glass surface in the flow cell to allow microtubules to be visualized. Scale bar, 10 μm. Full scans of the SDS–PAGE gels are provided in Supplementary Information, Figs S3, S4.

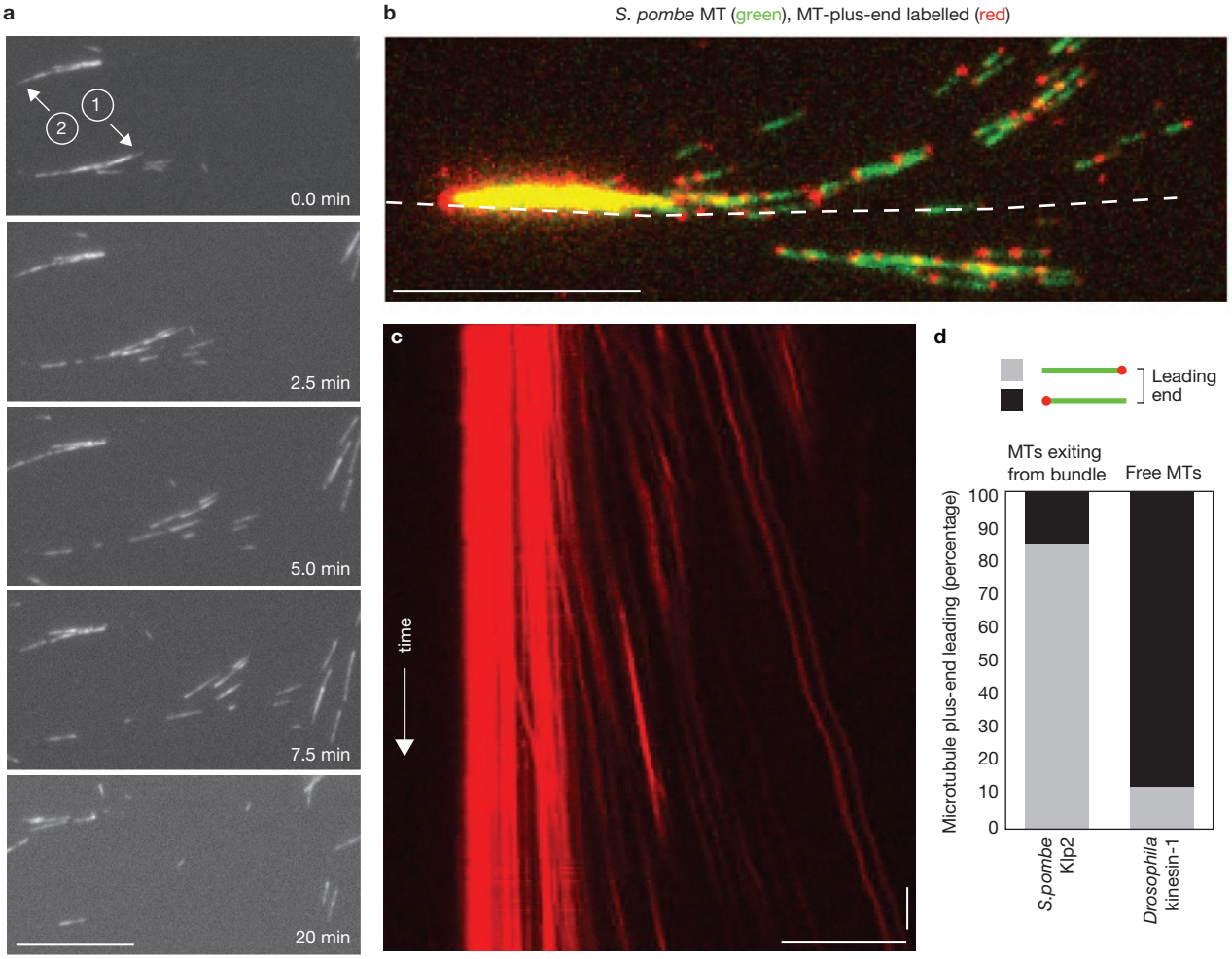

Figure 3 Full-length Klp2 organizes *S. pombe* microtubules into parallel bundles. (**a**) Microtubule gliding assay using microtubules assembled from *S. pombe* EGFP–tubulin (green) in PEM100 plus 100 mM NaCl. We note that surface binding is mediated by the population of Klp2 that was not microtubule-bound (see pelleting assay Fig. 2c, lane 1), in addition to motors attached to the bundles. Two bundles are shown (1 and 2) dispersing. Note that $t = 0$ is the time-point 20 min after motors and microtubules were mixed together. Scale bar, 10 μm. (**b**) Microtubule gliding assay using polarity-marked *S. pombe* microtubules (MT, 200 nM) which were premixed with 100 nM full-length Klp2 in solution (PEM100 plus 42 mM NaCl) and then added to the flow cell. The image shows the position of microtubules at the first time-point. Scale bar, 10 μm. (**c**) Kymograph analysis based on the dotted white line in **b**. Time is on the *y* axis with the vertical bar indicating 1 min and horizontal scale bar, 10 μm. (**d**) Quantification of microtubule gliding events using full-length Klp2 (minus-end directed motor; $n = 32$) or *Drosophila* kinesin-1 (plus-end-directed motor; $n = 38$). Shown are the percentages of gliding microtubules with a single leading (grey) or lagging (black) rhodamine-labelled end.

indicates that there is a specific binding site for the tail on each tubulin heterodimer or possibly between adjacent heterodimers.

We next asked whether the two microtubule binding sites in full-length Klp2 (motor domain and tail region) could support the formation of lateral contacts between microtubules and, in turn, microtubule bundling. We therefore mixed 100 nM full-length Klp2 with 200 nM *S. pombe* EGFP-labelled microtubules in solution (PEM100 plus 100mM NaCl) and incubated them for 20 min. This mixture was then added to a flow cell and bundles visualized as the motor–microtubule complexes bound to the glass surface. This experiment revealed that full-length Klp2 promoted the formation of *S. pombe* microtubule bundles (Fig. 2i, third panel). The extent of bundle formation depended on the Klp2 concentration: reducing the Klp2 protein concentration (20–50 nM) produced a reduction in bundles and an increase in free microtubules, whereas increasing the concentration to 200 nM produced larger bundle structures (Fig. 2i). When these experiments were carried out with a mixture of pig brain and *S. pombe* microtubules (both at 200 nM) and full-length Klp2 (100 nM), we also observed combined *S. pombe*/pig brain microtubule bundles (Supplementary Information, Fig. S1b). Crucially, neither Klp2-tail or Klp2-motor domain proteins (both at 100 nM) were able to drive bundle formation (Fig. 2j, second and third panels). These data demonstrate that the formation of microtubule bundles requires microtubule binding by both the motor-head and the tail domain of Klp2.

To investigate the organization of the microtubule bundles we took advantage of the classic microtubule-gliding assay. We mixed 100 nM full-length Klp2 with 200 nM EGFP-labelled *S. pombe* microtubules in solution and after 20 min added the mixture to a flow cell. We observed that in the presence of ATP, single microtubules were pulled out of those bundles that landed on the surface-attached Klp2 kinesins, demonstrating that the bundles could be 'unlocked' by an imbalance of Klp2-generated force. All microtubules moved uni-directionally, initially sliding in parallel, and subsequently tending to splay apart until

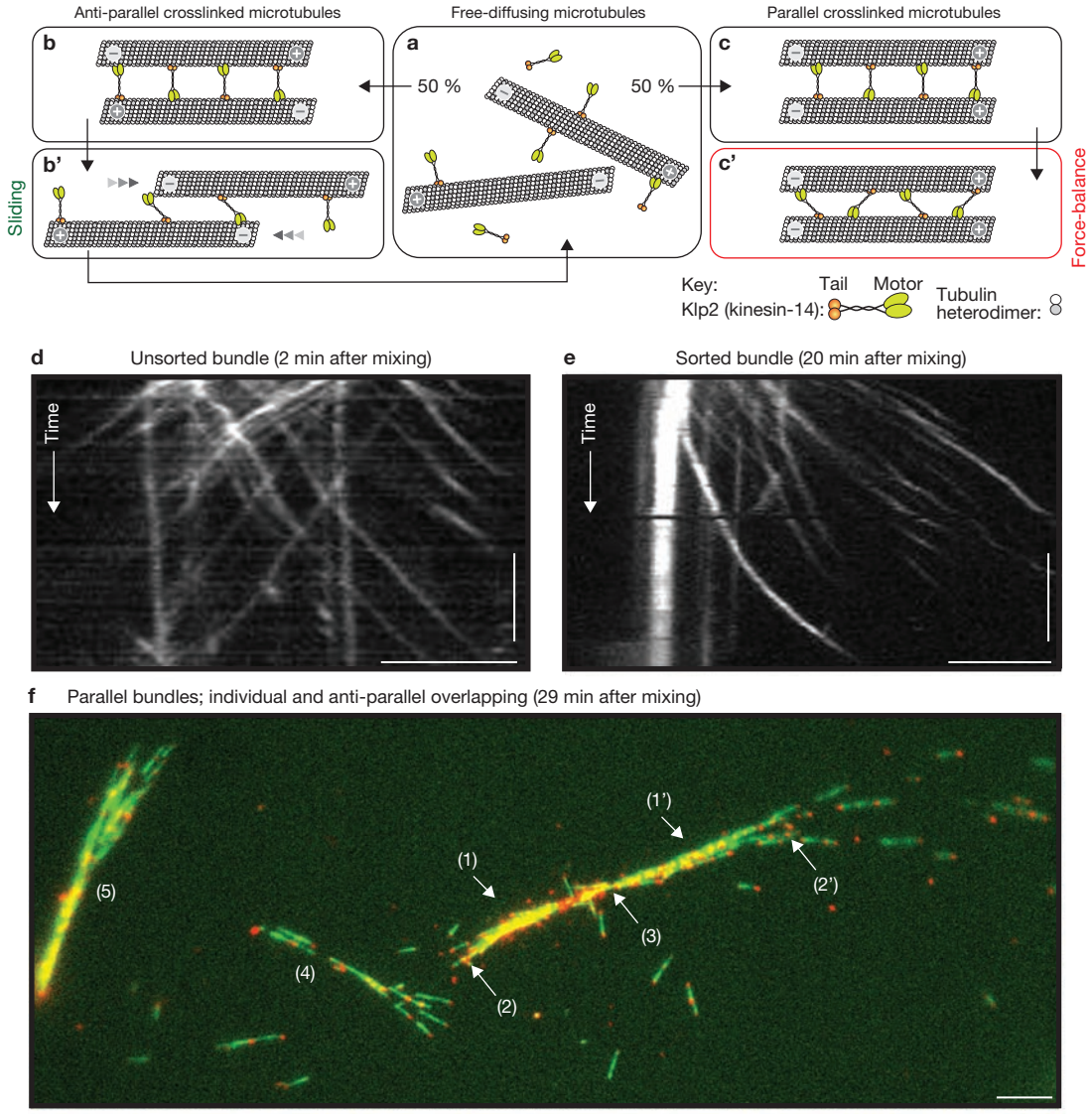

Figure 4 Force-balance model for motorized microtubule sorting. (**a**–**c**) Klp2 motors freely diffusing in solution bind to microtubules through interactions with the motor (yellow ovals) and tail (orange circles) domain (**a**). Klp2 motors thus establish lateral crosslinks between diffusing microtubules at random, leading to a mixture of anti-parallel (**b**) and parallel (**c**) overlapping microtubules. (**b**′) Klp2 causes anti-parallel overlapped microtubules to slide apart, leading to a full dissociation of the microtubules (direction of sliding microtubules is indicated by arrowheads) (**c**′) Parallel-overlapped microtubules are selectively trapped by the force-balance of the oppositely attached sets of Klp2 motors. (**d**, **e**) Kymographs from microtubule gliding assay using polarity-marked *S. pombe* microtubules (200 nM), which were premixed with 100 nM full-length Klp2 in solution (PEM100 plus 100 mM NaCl) and then added to the flow cell after 2 min (**d**) or 20 min (**e**). Time is on the *y* axis with the vertical bar indicating 5 min. Horizontal scale bar, 5 μm. (**f**) Image of a microtubule array at t = 9 min (29 min after mixing microtubules and motors in PEM100 plus 42 mM NaCl) from Supplementary Information, Movie 6, which is composed from two parallel microtubule bundles (1 and 1′). Each bundle contains microtubules with their plus-ends exclusively orientated towards the distal ends of the array (2 and 2′), and overlap in an antiparallel zone (3). Also visible are two parallel bundles (4 and 5). Scale bar, 10 μm.

the entire bundle disassembled (Fig. 3a; Supplementary Information, Movie 2). To further confirm this, we generated polarity-marked *S. pombe* microtubules. To do this, microtubules were first polymerized from GFP-labelled *S. pombe* tubulin and then capped with rhodamine-labelled pig brain tubulin. This resulted in a microtubule population in which about 30% had a single red mark at one end (the rest had multiple marks, presumably resulting from fusion events between microtubules, and were removed from any analysis). In a gliding assay with the plus-end directed *Drosophila* kinesin-1, more than 85% of these microtubules moved with the non-labelled end leading as expected when the rhodamine-cap marks the microtubule plus-ends (Fig. 3d). We then mixed 100 nM Klp2 with 200 nM polarity-marked *S. pombe* microtubules in solution, incubated for 20 min and added the mixture to a flow cell. As expected, we observed bundles that landed on the surface with microtubules exiting the bundle uni-directionally (Fig. 3b; Supplementary Information, Movie 3). Of these microtubules pulled out of the bundle, 87.5% had the rhodamine-cap leading (Fig. 3d), confirming their parallel configuration. Kymograph analysis of the rhodamine caps from this movie again clearly shows microtubules exiting the bundle from the right-hand side, but not the left-hand side (Fig. 3c). This uni-directional sliding of microtubules out of the bundle unequivocally demonstrates that the bundles are composed exclusively of parallel microtubules.

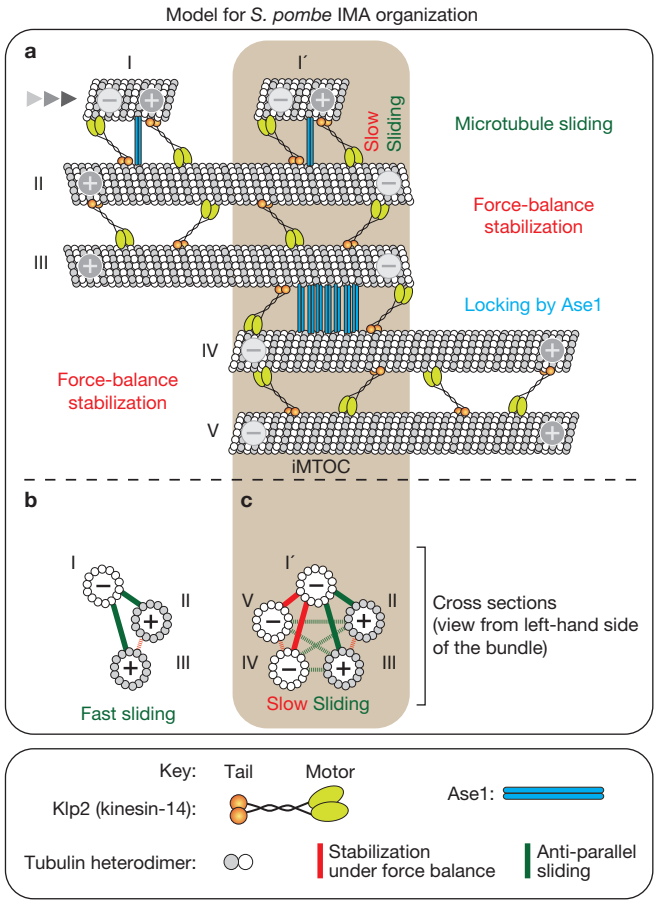

Figure 5 Model for the *S. pombe* interphase IMA organization. During dynamic IMA maintenance *in vivo,* assembled microtubules are incorporated into existing microtubule arrays. (**a**) We propose that microtubules (for example, II and III), which are in a parallel configuration, will be locked under force balance by Klp2. By contrast, a short microtubule (for example, I), which binds in an anti-parallel configuration with the IMA (for example, II and III), will slide to the centre of the cell. The force of the Klp2 motor is able to overcome the effect of Ase1 (blue bar), which has been shown to localize to these short microtubules *in vivo* and crosslink anti-parallel microtubules *in vitro.* (**b**) Cross-section of interactions between microtubule I, II and III: green lines indicate sliding and red lines stabilization under force balance. As microtubule I (now designated as microtubule I´) arrives at the antiparallel overlap zone within the IMA (iMTOC), Klp2 molecules can also now interact with parallel microtubules (for example, V and IV) and cause sliding to slow down. (**c**) Cross-section of interactions between microtubule I´, II, III, IV and V. At this point, the Ase1 molecules are able to overcome the reduced Klp2 sliding force and stabilize the iMTOC.

To explain our data we propose that Klp2 drives the formation of parallel bundles of *S. pombe* microtubules by a motorized sorting mechanism. In our model, free microtubules in solution (Fig. 4a) are first captured and crosslinked by Klp2 motor and tail domains. This initial capture phase results in an equal proportion of anti-parallel or parallel microtubule overlaps (Fig. 4b, c). In the presence of ATP, the motor activity of Klp2 then resolves these initial mixed-polarity bundles into a purely parallel arrangement: In the case of anti-parallel crosslinked microtubules, the Klp2 motor domains drive relative sliding apart of the crosslinked microtubules until they eventually dissociate (Fig. 4b´). By contrast, in the parallel geometry, all Klp2 kinesins attempt to move to the minus-end of the bundle, which causes the motors to stall under load. The forces produced by the two opposing sets of Klp2 motors balance and effectively cancel each other out (Fig. 4c´), stabilizing the structure in force-balance. Our data show that the parallel microtubule bundles generated *in vitro* are self-organized, energy dissipating structures (because of the requirement for ATP), which are stable under force-balance, yet can be readily destabilized through the application of external force, or by an imbalance of internal forces.

One prediction of our model is that repeated rounds of microtubule sliding, dissociation, and recapture are required for Klp2-dependent sorting to reach completion. To test this, we mixed Klp2-full length protein with *S. pombe* microtubules in solution and observed the formation of organized bundles by removing a sample at 2 min and then at 20 min. As predicted, we observed anti-parallel microtubules within the evolving bundle structure at the 2 min time-point: the kymograph of rhodamine caps clearly shows the movement of microtubules in both directions within the bundle structure, indicating an unsorted bundle (Fig. 4d; Supplementary Information, Movie 4). After 20 min incubation, we observed parallel structures, with microtubules all moving in the same direction as they exit the bundle (Fig. 4e; Supplementary Information, Movie 5). At the same time we also observed the presence of structures composed of two parallel bundles that were joined by a short overlap zone (Fig. 4f; Supplementary Information, Movie 6). We propose that such structures are intermediates between unsorted and sorted bundles. These data support our model that Klp2 actively sorts microtubules into organized parallel bundles.

What inferences can we draw about the *in vivo* role of Klp2? Current models for IMA formation in *S. pombe* propose that Klp2 is required for the sliding of short microtubules into the overlap zone, and in controlling the proportion of anti-parallel overlaps, compared with parallel overlaps within the IMA[1,4]. Models from Tran, Nedelec, Nurse and colleagues postulate a role for plus-tip-bound Klp2 in sliding short anti-parallel microtubules along an IMA arm and into the mid-zone of the cell where they are locked in place by Ase1, a protein that recognizes and specifically stabilizes anti-parallel overlaps[4]. Our new data are consistent with, and complimentary to, this proposal. Our *in vitro* data show that Klp2 binds along the lattice of *S. pombe* microtubules, where it drives antiparallel-overlapped microtubules to slide apart, while stabilizing parallel overlaps. Consistent with this model, we could observe that Klp2–GFP is localized to both microtubule plus-ends and the microtubule lattice in *S. pombe* cells (Supplementary Information, Movie 7). We now propose a synthesis of these two models, in which lattice-bound Klp2 slides short anti-parallel-overlapped microtubules into the mid-zone, where their anti-parallel overlap with the opposing IMA arm is stabilized by Ase1, and the parallel overlap of the newly arrived microtubule with the opposing IMA arm is stabilized by Klp2 (Fig. 5). This new model is consistent with observations that deletion of *ASE1* still allows microtubule bundling to take place, but overlapping regions are unstable[3,17].

What are the general implications of our results? Our data identify a robust mechanism for the motor-driven self-organization of microtubules into parallel bundles. Consistent with this, work from Diez and colleagues have directly demonstrated using a microtubule–microtubule sliding assay that another kinesin-14 (*Drosophila* Ncd), can slide apart pairs of anti-parallel microtubules but locks together parallel ones (see Fink *et al.,* this issue of *Nature Cell Biology*). Eg5, the *Xenopus* homotetrameric microtubule plus-end-directed kinesin-5, has previously been reported to slide antiparallel- but lock parallel microtubules[18,19]. This suggests the possibility that

a sorting mechanism similar to that described here may be conserved in both kinesin-14 and kinesin-5. We therefore expect that the mechanisms defined in our force-balance model will have a fundamental role in the establishment of complex cellular microtubule-based structures such as the IMA and bipolar spindles. The dynamic organization of microtubule arrays driven by molecular motors, in contrast to passive crosslinking of microtubules by MAPs (microtubule associated proteins), has the advantage that microtubule-based structures can be rapidly readjusted, as we have shown, by tipping of the force-balance. To fully test the implications of these ideas it will be crucial to develop an *in vitro* reconstitution assay that faithfully recapitulates the combination of microtubule dynamics, modulated by MAPs and molecular motors, and the self-organization of assembled microtubules mediated by MAPs, and sliding driven by molecular motors, these being distinct but complementary strategies that eukaryotic cells use to control and adjust the structure of their microtubule cytoskeleton.

Note added in proof: a related manuscript by Diez et al. *(*Nature Cell Biol. ***11,*** *doi:10.1038/ncb1877; 2009) is also published in this issue.*

METHODS

Methods and any associated references are available in the online version of the paper at http://www.nature.com/naturecellbiology/

Note: Supplementary Information is available on the Nature Cell Biology website.

ACKNOWLEDGEMENTS

We thank Joe Howard for the full-length *Drosophila* kinesin-1 construct and Michael Osei for purification of *S. pombe* tubulin and EGFP–tubulin. This work was supported by Marie Curie Cancer Care (A.D.M. and R.A.C.) and the Medical Research Council (R.A.C.).

AUTHOR CONTRIBUTIONS

M.B. conceived, designed and performed the experiments, and contributed to the writing of this study; D.R.D. created *S. pombe* strains, developed the methodology for purification of *S. pombe* tubulin and helped write the manuscript; A.D.M. and R.A.C. designed experiments and wrote the manuscript.

COMPETING FINANCIAL INTERESTS

The authors declare no competing financial interests.

Published online at http://www.nature.com/naturecellbiology/
Reprints and permissions information is available online at http://npg.nature.com/reprintsandpermissions/

1. Carazo-Salas, R. E., Antony, C. & Nurse, P. The kinesin Klp2 mediates polarization of interphase microtubules in fission yeast. *Science* 309, 297–300 (2005).
2. Carazo-Salas, R. E. & Nurse, P. Self-organization of interphase microtubule arrays in fission yeast. *Nature Cell Biol.* 8, 1102–1107 (2006).
3. Daga, R. R., Lee, K. G., Bratman, S., Salas-Pino, S. & Chang, F. Self-organization of microtubule bundles in anucleate fission yeast cells. *Nature Cell Biol.* 8, 1108–1113 (2006).
4. Janson, M. E. *et al.* Crosslinkers and motors organize dynamic microtubules to form stable bipolar arrays in fission yeast. *Cell* 128, 357–368 (2007).
5. Gadde, S. & Heald, R. Mechanisms and molecules of the mitotic spindle. *Curr. Biol.* 14, 797–805 (2004).
6. Broussard, J. A., Webb, D. J. & Kaverina, I. Asymmetric focal adhesion disassembly in motile cells. *Curr. Opin. Cell Biol.* 20, 85–90 (2008).
7. Nedelec, F. J., Surrey, T. & Karsenti, E. Self-organisation and forces in the microtubule cytoskeleton. *Curr. Opin. Cell Biol.* 15, 118–124 (2003).
8. Ehrhardt, D. W. Straighten up and fly right: microtubule dynamics and organization of non-centrosomal arrays in higher plants. *Curr. Opin. Cell Biol.* 20, 107–116 (2008).
9. Surrey, T., Nedelec, F. J., Leibler, S. & Karsenti, E. Physical properties determining self-organization of motors and microtubules. *Science* 292, 1167–1171 (2001).
10. Hagan, I. M. The fission yeast microtubule cytoskeleton. *J. Cell Sci.* 111, 1603–1612 (1998).
11. Brunner, D. & Nurse, P. New concepts in fission yeast morphogenesis. *Philos. Trans. R. Soc. Lond. B. Biol. Sci.* 355, 873–877 (2000).
12. Drummond, D. R. & Cross, R. A. Dynamics of interphase microtubules in *Schizosaccharomyces pombe*. *Curr. Biol.* 10, 766–775 (2000).
13. Hoog, J. L. *et al.* Organization of interphase microtubules in fission yeast analyzed by electron tomography. *Dev. Cell* 12, 349–361 (2007).
14. Alonso, M. C. *et al.* An ATP gate controls tubulin binding by the tethered head of kinesin-1. *Science* 316, 120–123 (2007).
15. Karabay, A. & Walker, R. A. Identification of microtubule binding sites in the Ncd tail domain. *Biochemistry* 38, 1838–1849 (1999).
16. Wendt, T. *et al.* A structural analysis of the interaction between ncd tail and tubulin protofilaments. *J. Mol. Biol.* 333, 541–552 (2003).
17. Loiodice, I. *et al.* Ase1p organizes antiparallel microtubule arrays during interphase and mitosis in fission yeast. *Mol. Biol. Cell* 16, 1756–1768 (2005).
18. Kapitein, L. C. *et al.* The bipolar mitotic kinesin Eg5 moves on both microtubules that it crosslinks. *Nature* 435, 114–118 (2005).
19. Uteng, M., Hentrich, C., Miura, K., Bieling, P. & Surrey, T. Poleward transport of Eg5 by dynein–dynactin in *Xenopus laevis* egg extract spindles. *J. Cell Biol.* 182, 715–726 (2008).
20. Gulick, A. M., Song, H., Endow, S. A. & Rayment, I. X-ray crystal structure of the yeast Kar3 motor domain complexed with Mg.ADP to 2.3 A resolution. *Biochemistry* 37, 1769–1776 (1998).
21. Lupas, A., Van Dyke, M. & Stock, J. Predicting coiled coils from protein sequences. *Science* 252, 1162–1164 (1991).
22. Hackney, D. D. Implications of diffusion-controlled limit for processivity of dimeric kinesin head domains. *Biophys. J.* **68,** 267S–270S (1995).

METHODS

Protein purification. The 6xHis-tagged full-length Klp2 (amino acids 1–817), Klp2 motor domain (Klp2-motor; amino acids 356–817) and Klp2 coiled coil plus tail domain (Klp2-tail; amino acids 1–634) were generated as described in the Supplementary Information, Methods. The full-length *Drosophila* kinesin-1 heavy chain was expressed and purified as described in the Supplementary Information, Methods.

***S. pombe* tubulin.** We created an *S. pombe* strain mmsp174 (*h⁻ura4.d18 arg3.D4 atb2⁻::nda2⁺*) containing only α1- and β-tubulin protein isoforms by replacing the *atb2* (α2) gene protein-encoding region with the protein-encoding region of the α1 gene *nda2*, using a DNA fragment PCR-amplified from genomic DNA and a previously described method for gene replacement in yeast[23]. Single isoform *S. pombe* α1 and β-tubulin was prepared from an 80 l culture of cells grown in a fermenter, collected by centrifugation and frozen in liquid nitrogen (Large Scale Laboratory, NIMR, London). The cell pellet was processed as described previously[24] with the addition of a polymerization and depolymerization cycle then gel filtration on Superdex 200 before the purified tubulins were desalted into PEMICO buffer[25] (100 mM PIPES, 1 mM $MgSO_4$ and 2 mM EGTA adjusted to pH 6.9 with KOH) containing 20 μM GDP, concentrated in a spin concentrator and stored in liquid nitrogen. Protein concentrations were determined by UV-absorption scan of protein samples dissolved in guanidine hydrochloride (6 M), assuming full nucleotide occupancy and ε of 108,390 M^{-1} cm^{-1}. GFP-labelled tubulin was prepared by the same method from the *S. pombe* strain mmsp33 (ref. 12), which contains α1β, α2β and EGFP–α1β tubulin heterodimers. The EGFP–α1β tubulin forms 13% of the total purified tubulin heterodimers. Both *S. pombe* tubulin preparations had a purity of 98%, as determined by Sypro Red fluorescence dye staining of SDS–PAGE gels loaded with 10ug of tubulin. Gels were imaged using an FX ProPlus Molecular Imager (Bio-Rad) and quantified using Quantity One software (Bio-Rad).

Protein biochemistry. Size exclusion chromatography and glycerol gradients were performed as described previously[26], except that we used PEM100 (100 mM Pipes pH 6.9, 2 mM EGTA, 1 mM $MgCl_2$) plus 100 mM NaCl and 10 mM β-mercaptoethanol.

Biochemical assays. The steady-state ATPase assay was performed as described previously[18] except that we used PEM100, 100 mM NaCl, 10 mM β-mercaptoethanol buffer. Microtubule pelleting assays were performed as described previously[27] and quantified using the Sypro Red fluorescence dye staining method described above. All assays, including microtubule gliding, were carried out at 25 °C.

***S. pombe* microtubules.** *S. pombe* microtubules were assembled from *S. pombe* tubulin (5 μM) in PEM100, 1 mM GMP–CPP for 1 h at 4 °C and then 1.5 h at 30 °C. Note that *S. pombe* microtubules cannot be stabilized with paclitaxel; therefore GMP–CPP was used which leads to more nucleation events, and subsequently more numerous but shorter microtubules at a given tubulin concentration. To generate plus-end labels, EGFP–*S. pombe* microtubules polymerized from 5 μM tubulin were incubated with 0.4 μM N-ethylmaleimide-modified pig-brain tubulin and 0.8 μM rhodamine-labelled bovine brain tubulin (Cytoskeleton) in PEM100, 1 mM GMP–CPP for 30 min at 30 °C. The capped microtubules were pelleted, resuspended in PEM100, 1 mM GMP-CPP, 20 μM paclitaxel, and stored at 30 °C. Pig-brain microtubule polymerization is described in the Supplementary Information, Methods.

Microtubule gliding assay. Microtubules and Klp2 proteins were premixed and incubated at 25 °C in PEM100, 100 mM NaCl, 10 mM β-mercaptoethanol, 10 mg ml^{-1} BSA and 20 μM paclitaxel, 1 mM GMP-CPP, 4 mM ATP, Oxygen scavenger (20 mM glucose, 0.2 mg ml^{-1} catalase, 0.4 mg ml^{-1} glucose oxidase) and an ATP regeneration system (10 mM phosphocreatine, 50 μg ml^{-1} creatine phosphate-kinase). The assay mix was then flowed into the chamber and frames acquired every 3 s using a ×60 oil NA 1.4 objective on a Olympus DeltaVision RT (API) equipped with a DAPI-FITC-Rhod/TR-Cy5 filter set (Chroma) and a Coolsnap HQ camera.

23. Erdeniz, N., Mortensen, U. H. & Rothstein, R. Cloning-free PCR-based allele replacement methods. *Genome Res.* **7,** 1174–1183 (1997).
24. Davis, A., Sage, C. R., Wilson, L. & Farrell, K. W. Purification and biochemical characterization of tubulin from the budding yeast *Saccharomyces cerevisiae*. *Biochemistry* **32,** 8823–8835 (1993).
25. Walker, R. A. *et al.* Dynamic instability of individual microtubules analyzed by video light microscopy: rate constants and transition frequencies. *J. Cell Biol.* **107,** 1437–1448 (1988).
26. McClelland, S. E. *et al.* The CENP-A NAC/CAD kinetochore complex controls chromosome congression and spindle bipolarity. *EMBO J.* **26,** 5033–5047 (2007).
27. Lockhart, A. & Cross, R. A. Origins of reversed directionality in the ncd molecular motor. *EMBO J.* **13,** 751–757 (1994).

nature cell biology

DOI: 10.1038/ncb1878

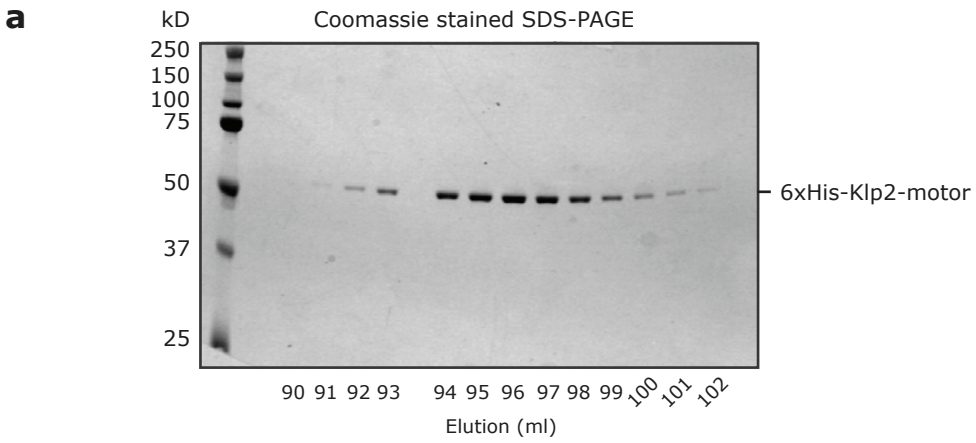

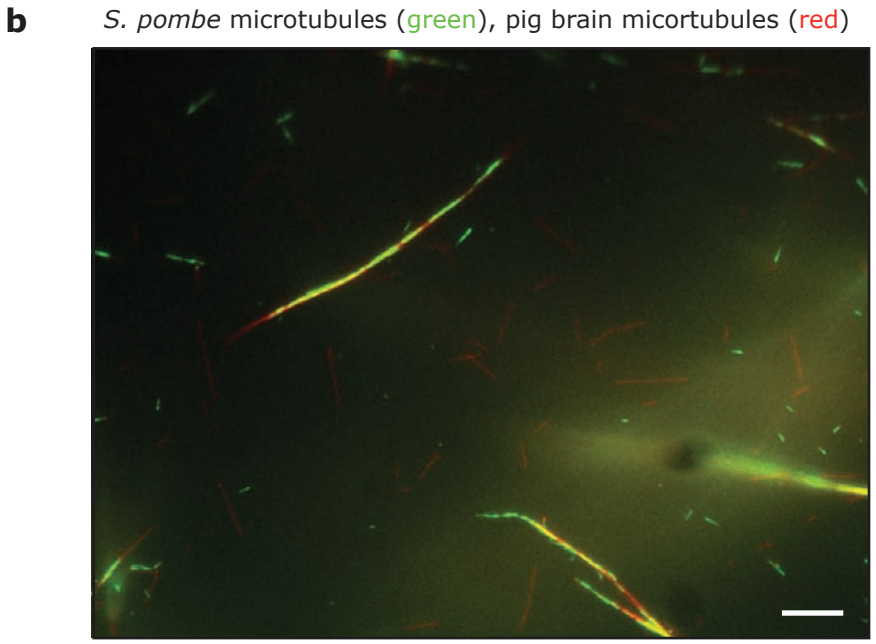

Figure S1 a, Fractions of the single-peak elution from the size exclusion chromatography of the purified Klp2-motor protein performed in PEM100 plus 100 mM NaCl. Note that the A_{280} trace showed no proteins eluting at any other positions on the column. The measured stokes radius for the Klp2-motor was 47Å, consistent with a homodimeric species. **b,** Representative images of the microtubule-motor structures that formed after 20 mins when Klp2-full length (100 nM) was mixed with 200 nM of *S. pombe* EGFP-microtubules and 200 nM Rhodamine-labelled pig-brain microtubules (PEM100 plus 100 mM NaCl, pH6.8) and the mixture added to a flow cell. Scale bar = 10 μm.

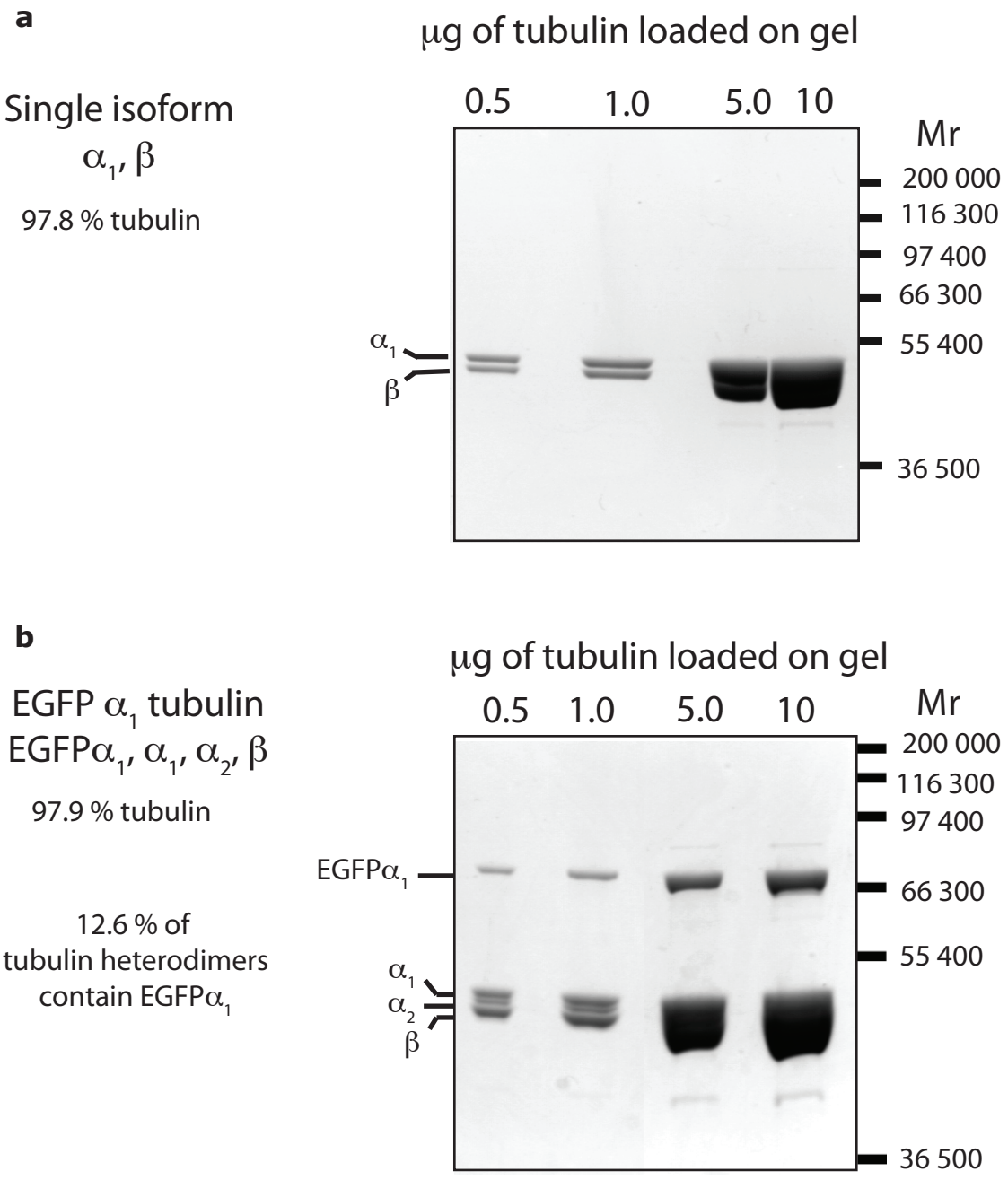

Figure S2 Coomassie stained SDS-PAGE of purified *S. pombe* tubulin **a,** Single isoform *S. pombe* tubulin and **b,** EGFPα_1 tubulin. This corresponds to Fig. 2b.

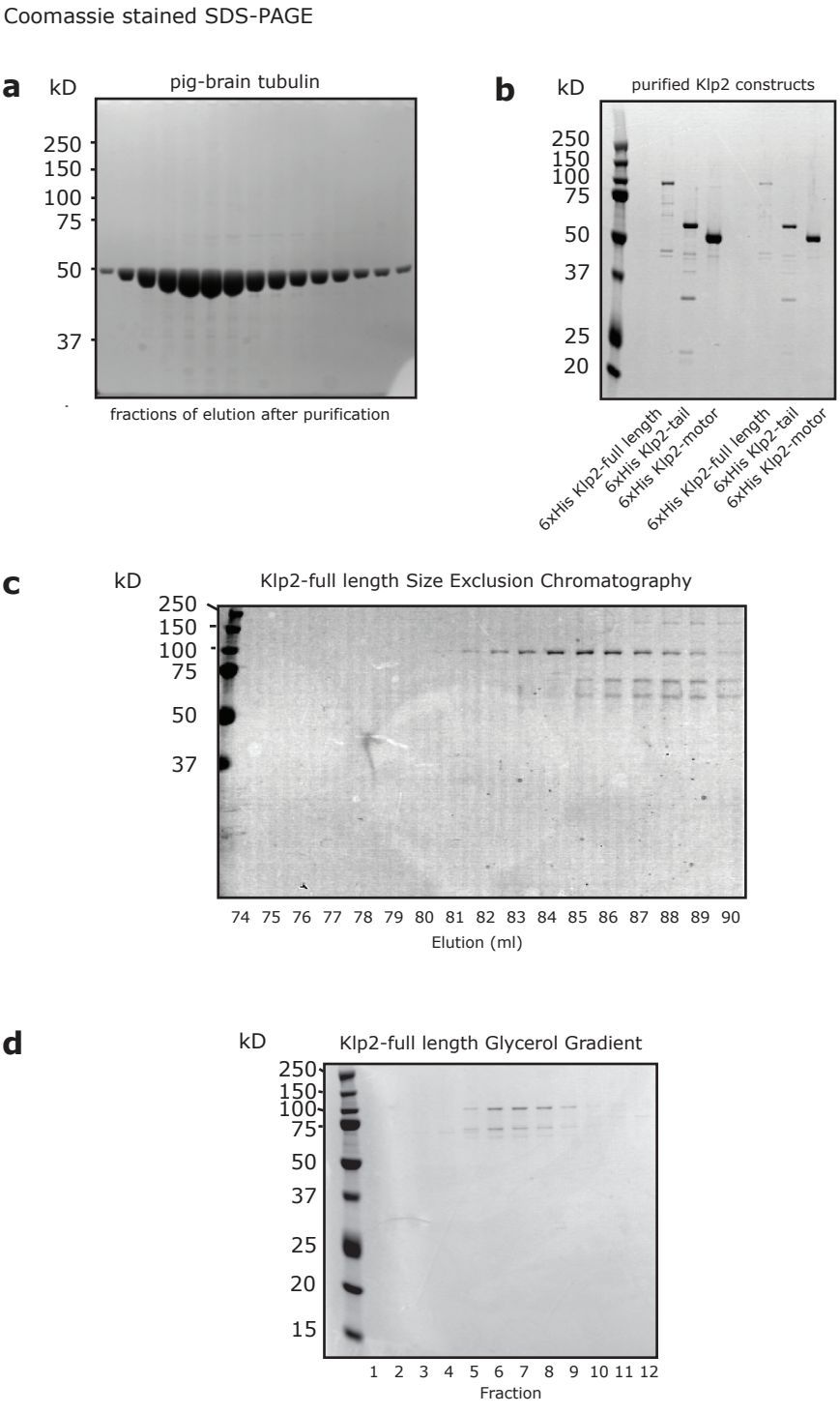

Figure S3 Coomassie stained SDS-PAGE of **a,** Purified pig-brain tubulin (corresponds to Fig. 1f) **b,** Purified Klp2 recombinant protein constructs (corresponds to Fig. 2b) **c,** Full-length Klp2 size exclusion chromatography (corresponds to Fig. 1d, upper panel) and **d,** Full-length Klp2 glycerol gradient (corresponds to Fig. 1d, lower panel).

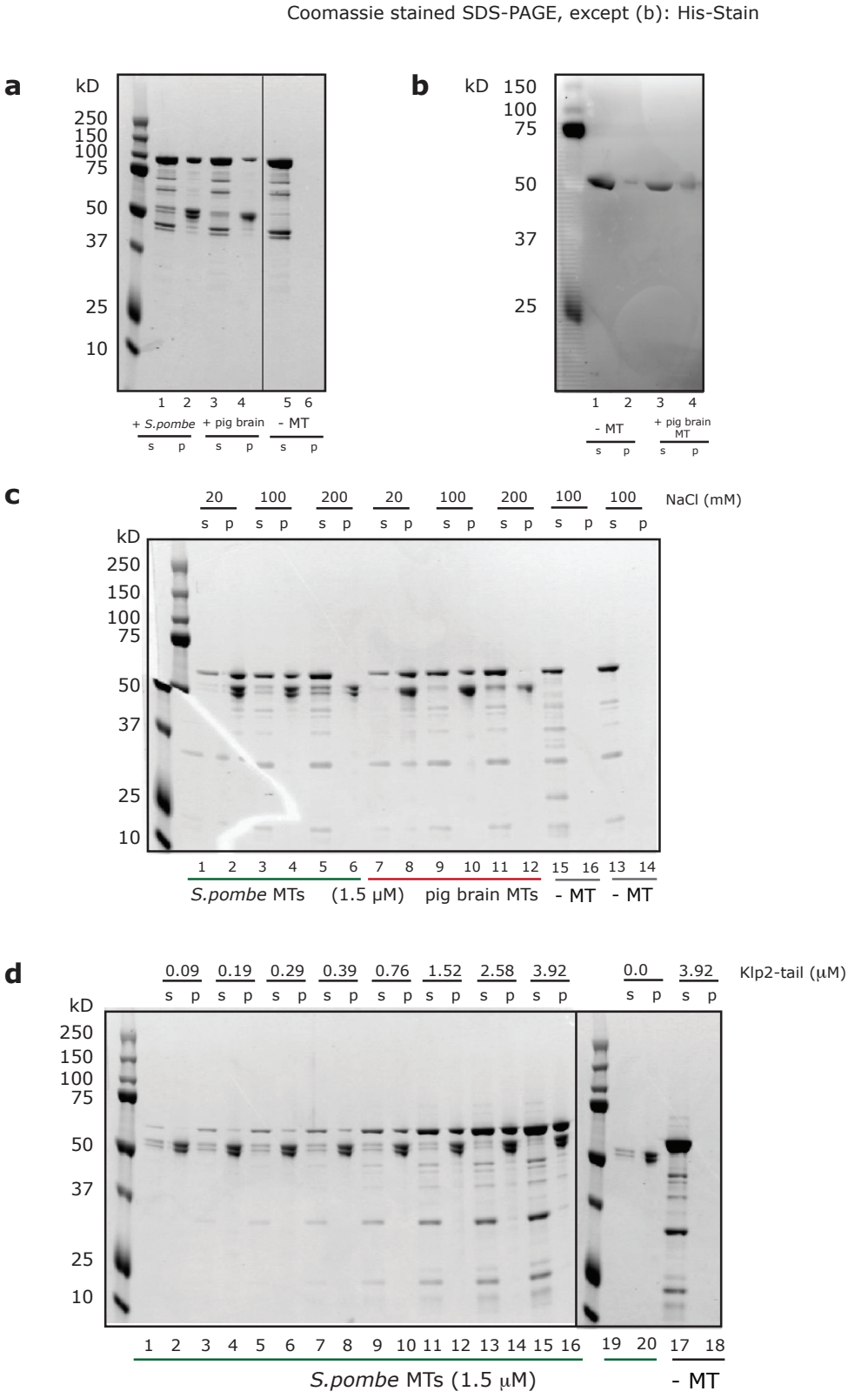

Figure S4 Microtubule co-pelleting assays, SDS-PAGE stained with His-stain **b,** Klp2-motor (corresponds to Fig. 2d), or Coomassie **a,** Full-length Klp2 (corresponds to Fig. 2c), **c,** Klp2-tail, ionic strength dependent binding, (corresponds to Fig. 2e) and **d,** Klp2-tail titration (corresponds to Fig. 2g).

Supplementary Movie Legends
Time-lapse and scale as indicated in the movies.

Movie S1 Microtubule gliding assay using polarity-marked rhodamine-labaled pig brain microtubules showing that full length Klp2 is a minus-end directed molecular motor protein.

Movie S2 Microtubule gliding assay using polarity-marked *S. pombe* EGFP microtubules (only the green, EGFP channel is shown). The dispersion of two parallel microtubule bundles is shown. Note that the microtubules all move uni-directionaly out of the bundle structure, which fully disperses during the course of the movie showing that all microtubules were parallel. This movie corresponds to Fig. 3a.

Movie S3 Microtubule gliding assay using polarity-marked *S. pombe* EGFP microtubules showing the dispersion of a parallel microtubule bundle. Both the EGFP channel (microtubules) and Rhodamine channel (Paclitaxel stabilized Rhodamine-labelled pig brain tubulin – microtubule plus-end caps) are shown. Note that the microtubules all move uni-directionaly out of the bundle structure. This movie corresponds to Fig. 3b.

Movie S4 Microtubule gliding assay using polarity-marked *S. pombe* EGFP microtubules showing the dispersion of a non-parallel unsorted microtubule bundle. Both the EGFP channel (microtubules) and Rhodamine channel (taxol stabilized Rhodamine-labelled pig brain tubulin) are shown. Note that the microtubules move in both directions within the bundle structure. This movie corresponds to Fig. 4d.

Movie S5 Microtubule gliding assay using polarity-marked *S. pombe* EGFP microtubules showing the dispersion of a parallel microtubule bundle. Both the EGFP channel (microtubules) and Rhodamine channel (taxol stabilized Rhodamine-labelled pig brain tubulin) are shown. Note that the microtubules all move uni-directionaly out of the bundle structure. This movie corresponds to Fig. 3e.

Movie S6 Microtubule gliding assay using polarity-marked *S. pombe* EGFP microtubules showing the dispersion of a parallel microtubule bundle. Microtubules and Klp2 motors were mixed in solution and then added to a flow cell at T=9 min. At the start the movie a microtubule array composed of two parallel microtubule bundles is visible in the centre of the field. Each bundle contains microtubules with their plus-ends exclusively orientated towards the distal ends of the array. After 2 min, and then 3 min, additional bundles land on the surface. These are both parallel bundles (now to the left of the large array) that disperse during the course of the movie. This movie corresponds to Fig. 4f and both the EGFP channel (microtubules; green) and Rhodamine channel (Paclitaxel stabilized Rhodamine-labelled pig brain tubulin; red) are shown.

Movie S7 Representative movie of Klp2-GFP (green) localization in living *S. pombe* cells. Movie showing stack of frames through the z-axis (step size = 0.2 μm). Note the localization of Klp2-GFP to bright foci as previously described (Janson et al., 2007) which represent the microtubule plus-ends. In addition, Klp2-GFP signal is clearly visible along the microtubule demonstrating that Klp2 is not restricted to only plus-ends, but also binds the microtubule lattice in *S. pombe* cells.

Supplementary Methods

Klp2 purification. Full-length *KLP2* cDNA was PCR amplified from a *S. pombe* cDNA library and cloned into the pET-28a(+) expression vector (Novagen). Deletion constructs were subcloned from that vector. The recombinant N-terminal hexa-histidine tagged fusion proteins were expressed in *E. coli* BL21-CodonPlus®(DE3)-RIPL Competent Cells (Stratagene) induced with 0.5 mM IPTG for 16 h at 15 °C. Harvested cells were resuspended in buffer A (50 mM sodium phosphate buffer pH 7.4, 2 mM $MgCl_2$, 10 mM 2-Mercaptoethanol, 0.1 mM ATP containing 50 mM NaCl and protease inhibitors (Roche), and lysed in 0.05 % vol/vol Triton X-100 (Sigma) and 0.1 mg/ml Lysozyme (Sigma) for 30 min at 4 °C. Cleared lysates were precipitated by adding 0.404 g/ml Ammonium sulfate (Sigma) and incubating for 1 h at 4 °C. The spun down pellet was resuspended in buffer A containing 300 mM NaCl, 10 mM ATP, 10 mM $MgCl_2$, 1 % vol/vol CHAPS (Sigma and protease inhibitors (Roche) and loaded onto a HisTrapHP column (GE Healthcare). The column was washed with buffer A containing 300 mM NaCl and 20 mM imidazole. Proteins were eluted in buffer A containing 300 mM NaCl and 85 mM imidazole; then desalted into PEM100, 100 mM NaCl, 10 mM β-mercaptoethanol, and snap-frozen in liquid nitrogen. Drosophila kinesin-1 was purified using the same method.

Rhodamine labeled pig-brain microtubules. Microtubules were either polymerized at 5 μM pig-brain tubulin, 0.6 μM rhodamin-labeled bovine-brain tubulin in PEM100, 1 mM GMP-CPP for 1.5 h at 30 °C or at 38 μM pig-brain tubulin in PEM100, 1 mM GTP for 20 min at 37 °C and then stabilized with 20 μM paclitaxel. Minus-end labeled pig-brain microtubules were generated by first polymerizing microtubule seeds from 20 μM pig-brain tubulin and 40 μM rhodamine-labeled bovine tubulin in PEM100, 1 mM GMP-CPP for 10 min at 37 °C. Then the seeds were diluted and microtubules polymerized at 23 μM pig-brain tubulin, 14 μM N-ethylmaleimide-modified pig-brain tubulin, 3.3 μM rhodamine-labeled bovine-brain tubulin in PEM100, 1 mM GTP and stabilized by the addition of 20 μM paclitaxel.

Flow chamber preparation. Coverslips were incubated in 10 M NaOH for ½ h and repeatedly sonicated together with slides (both Menzel Gläser) in detergent solution (2.8 ml/l Neutracon, Decon), followed each time by extensive rinsing with ddH_2O.

Flow chambers were assembled with < 0.5 mm grease as spacer resulting in 3 to 5 μl volume.

Gliding assay analysis. Raw data was processed by ImageJ software, microtubule movements were analyzed with the "MultipleKymograph' plug-in for ImageJ (http://www.embl.de/eamnet/html/body_kymograph.html). Average microtubule gliding velocities and standard deviations were obtained from velocity histograms generated from at least 50 microtubules.

Live cell imaging of *S. pombe* cells. *S. pombe* strain McI322 (*h- leu1 ura4 his-D1 ade6-210 klp2+-GFP-ura4+;* gift of Richard McIntosh) was grown under standard conditions. Cells were imaged at 26ºC on a Deltavision RT microscope using a 100x oil NA1.4 objective and an FITC filter set (API). Images were deconvoved using softworx software.